Parameterization of Water Electrooxidation Catalyzed by Metal Oxides Using Fourier Transformed Alternating Current Voltammetry

Shannon A. Bonke, Alan M. Bond, Leone Spiccia*, Alexandr N. Simonov*

School of Chemistry and the ARC Centre of Excellence for Electromaterials Science, Monash University, Victoria 3800, Australia

ABSTRACT: Detection and quantification of redox transformations involved in water oxidation electrocatalysis is often not possible using conventional techniques. Herein, use of large amplitude Fourier transformed a.c. voltammetry and comprehensive analysis of the higher harmonics has enabled us to access the redox processes responsible for catalysis. An examination of the voltammetric data for water oxidation in borate buffered solutions (pH 9.2) at electrodes functionalized with systematically varied low loadings of cobalt (CoO_x), manganese (MnO_x) and nickel oxides (NiO_x) has been undertaken, and extensive experiment-simulation comparisons have been introduced for the first time. Analysis shows that a single redox process controls the rate of catalysis for Co and Mn oxides, while two electron transfer events contribute in the Ni case. We apply a 'molecular catalysis' model that couples a redox transformation of a surface-confined species (effective reversible potential, E^0_{eff}) to a catalytic reaction with a substrate in solution (pseudo-first order rate constant, k^f_1), accounts for the important role of a Brønsted base, and reliably mimics the experimental behavior. The analysis revealed that E^0_{eff} for CoO_x, MnO_x and NiO_x lie within the range 1.9-2.1 V *vs.* reversible hydrogen electrode, and k^f_1 varies from 2×10^3 to 4×10^4 s^{-1}. The k^f_1 values are much higher than reported for any water electrooxidation catalyst before. The E^0_{eff} values provide a guide for *in situ* spectroscopic characterization of the active states involved in catalysis by metal oxides.

INTRODUCTION

The development of efficient chemical technologies needs to be underpinned by a detailed quantitative understanding of reaction mechanisms. One crucial technology receiving considerable attention nowadays is electrocatalytic water decomposition, as it would generate a clean and 'infinite' fuel, *viz.* molecular hydrogen.[1-3] The overall process includes cathodic hydrogen evolution and anodic oxygen evolution half-cell reactions, occurring under catalytic conditions.[4] The current view is that even for the most active catalytic materials, water oxidation (or the oxygen evolution reaction, OER) is still substantially less efficient than water reduction (the hydrogen evolution reaction).[5,6] This inefficiency has led to extensive searches for new catalysts, the recent focus being on materials derived from abundant elements that function efficiently in near-neutral or alkaline solutions. Catalysts addressing these requirements include Co,[7-11] Ni[12-14] and Mn[15-24] oxides/oxyhydroxides (CoO_x, NiO_x and MnO_x, respectively, and MO_x in general).

Linking these electrocatalysts together are structural similarities, with each composed of edge-sharing octahedral metal centers in a layered metal oxide arrangement.[13,15,17,24-32] These similarities have led to proposals that catalysis may be following a similar mechanism in each case.[5,33] Hence, CoO_x, NiO_x and MnO_x are the focus of the mechanistic study herein. Conveniently, facile oxidative electrodeposition methods are available to fabricate the MO_x-based water oxidation anodes.[7,10,12,16,18,34,35]

A substantial body of research on the mechanism of formation and catalytic function of electrodeposited metal oxides has been published in recent years, particularly for CoO_x. In these studies, CoO_x deposited from phosphate buffer is often denoted Co-P_i or Co-B_i for the borate equivalent,[7,8,34] to reflect the importance of the buffer in catalyst function, or more simply CoCat.[5,11] The Brønsted base is vital for efficient proton abstraction at each of four electron-transfer steps of water oxidation,[8,36,37] and mass-transport of base can limit the catalysis rather than the intrinsic reaction rates. Comprehensive electro-chemical[11,36-39] and spectroscopic[27,29,40] studies of CoO_x-catalyzed water electrooxidation have provided information on the rate-limiting steps. For example, Nocera and colleagues have proposed that proton-coupled $[Co^{III}\text{-}OH]/[Co^{IV}=O]$ electron transfer followed by slow oxygen-oxygen bond formation are the critical processes.[36]

More generalized insights into the mechanism of water oxidation have been provided through detailed density functional theory (DFT) calculations.[41-44] Examination of the water oxidation energetics indicates that key intermediates in the process (OH, O and OOH) are bound either too strongly or too weakly on all metal oxide surfaces. An implication of this is a significant intrinsic overpotential for water electrooxidation, which appears to be impossible to avoid for monometallic MO_x systems.

The mechanistic complexity of water electrooxidation is a main impediment to parameterization of the electron transfer and chemical transformation steps in this reaction. Nevertheless, several important contributions seeking to quantify the thermodynamics and kinetics have been reported recently. Ahn and Bard used scanning electrochemical microscopy to estimate apparent rate constants for the interaction of water with electrodeposited cobalt oxide.[45] Savéant and co-workers introduced fast scan rate d.c. cyclic voltammetry to study water electrooxidation catalyzed by CoO_x

and outlined the relevant theory,[46] while Dau and colleagues employed electrochemical impedance spectroscopy (EIS) to probe the kinetics of the MnO_x-catalyzed reaction.[32]

The present work aims to further advance the parameterization of the water oxidation mechanism *via* comparisons of experimental and simulated higher order harmonic data derived from Fourier transformed (FT) a.c. voltammetry. Advantages provided by the use of a.c. voltammetry for quantitative analysis of mechanisms where an electron transfer process is coupled to a chemical reaction[47] and in avoiding background current have been recently reported with surface confined processes.[48,49] To avoid the complicated electron/proton transport issues associated with thick catalyst films,[11,37,39,46] we have used very low surface concentrations of CoO_x, NiO_x and MnO_x immobilized on a low background electrode material.

EXPERIMENTAL

Materials. Reagent or analytical grade chemicals were used as received from commercial suppliers. Fluorine doped tin oxide (FTO) coated glass with a sheet resistance of 8 Ω square^{-1} was purchased from *Dyesol* (TEC8 Glass Plates). Reverse osmosis purified water (resistivity 1 MΩ cm at 25°C) was used to prepare all aqueous solutions. Borate buffer was prepared by alkalization of an aqueous boric acid solution with fresh 1 M NaOH.

Deposition Solutions. A 10 mM aqueous solution of $[CoEDTA]^{2-}$ was prepared as described previously,[10] and diluted with borate buffer (1:10) prior to the experiments. A λ_{max} at 467 nm (ε = 12 M^{-1} cm^{-1}) was determined by UV-Vis spectrophotometry (Lambda 950, *Perkin-Elmer*), consistent with literature.[50] The synthesis of $[Ni(NH_3)_6]Cl_2$ followed a published method[51] {λ_{max} = 568 nm (ε = 0.2 M^{-1} cm^{-1}), in agreement with literature[52]}. Aqueous solutions (0.5 mM) were prepared each day and diluted with borate buffer (1:50) to prepare the deposition solution. A stock solution of $[Mn(OH_2)_6]^{2+}$ (10 mM, aqueous) was prepared from $Mn(CH_3COO)_2{\cdot}4H_2O$ diluted with borate buffer (1:20) and used in deposition experiments.

Electrochemical Procedures. D.c. experiments were performed with a Bio-Logic VSP electrochemical workstation. Custom built instrumentation was used for the a.c. measurements.[53] All a.c. voltammetric experiments were undertaken with amplitude of ΔE = 0.08 V, which provides an adequate level of non-linearity to allow higher order harmonics to be detected, and at the same time, does not induce very significant ohmic losses and broadening.[53] The frequency of f = 9.02 Hz provides a sufficient level of kinetic sensitivity due to the relatively slow rates of the probed electron-transfer events (*vide infra*). Control experiments undertaken with f = 22.02 and 89.00 Hz did not allow enhanced a.c. current in higher order harmonics, which also confirms that 9.02 Hz was sufficient for analysis.

All experiments were undertaken in a three electrode configuration. Ag|AgCl|3 M NaCl (*BAS*) with a salt bridge was employed as the reference electrode, but potentials are reported *versus* the reversible hydrogen electrode (RHE; E_{RHE} / V = -0.21 - 0.059pH / V *vs.* Ag|AgCl). A custom made electrode positioner was used to maintain a constant distance between the working and reference electrodes, and the resistance between them (R_u) was quantified by EIS. The auxiliary electrode (high surface area Ti wire) was isolated from the test solution by a P4 glass frit (10-16 μm pore size). One cell was employed exclusively for electrocatalytic measurements, another for catalyst deposition to avoid contamination from metal oxide precursors. Only non-metallic items were used with the cells, *e.g.,* plastic tweezers to remove PTFE coated stirring bars. Prior to switching analysis to different cations, the cells were cleaned with hot aqua regia (HCl:HNO_3 3:1 vol.) and rinsed thoroughly with water.

The FTO glass used as a working electrode substrate was received as 100 × 100 mm sheets and laser-engraved (*Universal Laser Systems,* VLS3.50) to define the electroactive area (0.16 cm^2). The glass was then cut into rectangles (10 × 30 mm), and subjected to cleaning procedures (*vide infra*). Electrical connection was achieved by soldering a wire to the FTO electrode. The electroactive area was finally defined by polyimide (*Kapton*) tape to give the configuration shown in Fig. S1. Functionalization of FTO was performed by spontaneous adsorption of the MO_x precursor for the lowest loadings, voltammetrically for medium loadings and potentiostatically for the highest loadings.

Treatment of FTO Electrodes. Examination of water electrooxidation necessitates the use of an electrode substrate with negligible catalytic activity at up to *ca* 2 V *vs.* RHE. FTO subjected to standard cleaning procedures, *e.g.,* 20 min ultrasonications in surfactant (Hellmanex), water and ethanol (96%), displayed unwanted water oxidation activity (Fig. S2a), presumably due to traces of transition metal(s). To produce less catalytically active FTO (*magenta* traces in Fig. S2a), the electrodes were placed in $HNO_{3(aq)}$ (18 wt.%) and refluxed for 60 min or immersed in hot aqua regia for 10 min. Subsequently, the glass pieces were rinsed thoroughly under a stream of water. The water oxidation capacity could be further suppressed permanently by a single scan of the potential from 1.05 to -0.25 V *vs.* RHE (*teal* trace in Fig. S2a).

Inductively Coupled Plasma Mass Spectrometry (ICP-MS). Quantification of metal content of the deposited films was achieved by ICP-MS analysis (NexION 350D, *Perkin-Elmer*) of solutions obtained by dissolving MO_x in refluxing 4 M $HNO_{3(aq)}$ (CoO_x) or hot aqua regia (NiO_x, MnO_x) for 40-60 min, and resting for *ca* 16 h at ambient temperature. The values measured from three unused FTO electrodes were taken as a baseline. The samples were spiked with Sc internal standard, and a second internal standard of Y ions was plumbed into the sample inlet to allow correction for the instrumental drift. Raw analyte counts were standardized by means of a calibration curve constructed using commercially available stock solutions. No Fe contamination on the electrodes was detected. The exceptionally low dissolved metal ion concentrations were often at the limit of detection, which imposes a degree of uncertainty on some of the results.

THEORY

All simulations were undertaken with the DigiElch 7.F software.[54] The generally accepted water electrooxidation mechanism involves four proton-coupled electron transfer events,[42,43] whose modeling is challenging and requires several simplifying assumptions. The Butler-Volmer electron-transfer kinetics formalism, with charge-transfer coefficients arbitrarily set to 0.50, was used to avoid over-parameterization and ensuing uncertainties.[55,56] Use of Marcus-Hush theory could be more appropriate, but the required reorganization energies are not known.

Previous kinetic studies on water electrooxidation employed a so-called 'molecular catalysis' model.[32,45,46] Therein, water oxidation is proposed to occur *via* a chemical redox reaction between a substrate and a surface-confined catalyst when the latter reaches a sufficiently high oxidation state through application of a potential. By assuming that the rate-determining step in the 4-electron and 4-proton sequence is much slower than other three, the key reactions can be simplified to:

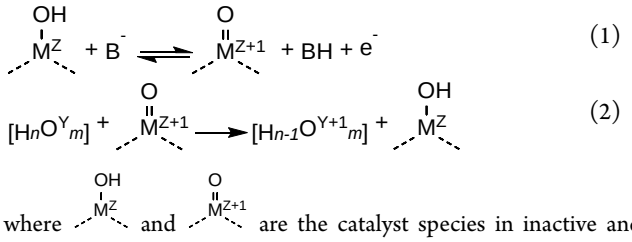

where and are the catalyst species in inactive and active (oxidized) state; B^- and BH are conjugate base of the buffer and its protonated form, respectively; $[H_nO^Y{}_m]$ and $[H_{n-1}O^{Y+1}{}_m]$ represent the reduced and oxidized states of the substrate at the rate-determining step.

In our analysis, the overpotential-determining process is assumed to occur first in the 4-electron transfer sequence, and the remaining three faster electron transfer steps are replaced with a hypothetical 3-electron process. This was necessary to facilitate simulations within the confines of the software package. The concentration of water is very high and can be assumed to remain constant at the electrode surface at all times. However, the process can still run into a mass-transport controlled regime, since each oxidation step requires withdrawal of a proton by a base (eq. 1). This was demonstrated previously,[46] and confirmed to apply here (Fig. S3). Thus, the reaction was assumed to be controlled by mass-transport of B^-, while the H_2O concentration was incorporated into relevant rate constants. Application of these assumptions leads to the simplified 'molecular catalysis' electrode model given in Table 1. The full set of parameters needed for simulation of this model is shown in Fig. S4.

The background currents from pre-treated FTO were very low within the potential ranges examined, but still needed to be included in the model. Modeling the faradaic part of this background response was undertaken using the mechanism in Table 1 and an arbitrary set of parameters (Fig. S4), while the non-faradaic background was simulated using a conventional constant C_{dl} model.[S6] Interestingly, our simulations predict that the presence of a more active catalyst (Co, Ni or Mn oxides) negates the contribution of the least active (FTO) (Fig. S5). From a broader perspective, the implication of this phenomenon is negligible benefit in performance from combining two catalysts on one water oxidation anode, unless there is a significant synergistic effect.

A more classical 'heterogeneous catalysis' water oxidation model was also briefly considered in our analysis. In this model, the reaction occurs *via* redox transformation of adsorbed species and the necessity for a catalyst to be oxidized to achieve an active state is not explicitly included (Table S1).[42,43] The major obstacles to undertaking comprehensive analysis with this model were software limitations, which allowed modeling using only a finite diffusion layer (akin to rapid stirring), while our experimental data were obtained in quiescent solutions. Nevertheless, when modeled under stirring conditions, the 'molecular' and 'heterogeneous' models can produce very similar voltammetric responses (Fig. S6). Thus, if needed, the parameters $[E^0_{cat}, k^0_{cat}, k^f]$ derived from our analysis based on the 'molecular catalysis' model, can be used to derive the corresponding $[K_{ads}, k^0_{het}, k^f_{ads}]$ parameters for the 'heterogeneous catalysis' model (see Table S1).

Table 1. 'Molecular catalysis' model of water electrooxidation used in simulations.

Reaction [a]		Parameters [b]
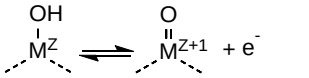	(3)	E^0_{cat} – unknown k^0_{cat} – unknown
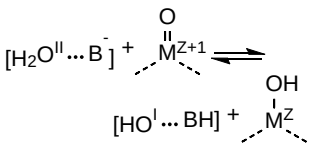	(4)[c]	k^f – unknown $K = \exp\left(F\left(E^0_{cat} - E^0_{lim}\right)/RT\right)$
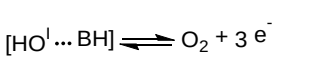	(5)[d]	$E^0_{non\text{-}lim}$ $k^0_{non\text{-}lim} >> k^0_{cat}$

[a] No specific chemical significance should be attached to the notation used. [b] E^0_{lim} and $E^0_{non\text{-}lim}$ were taken from Ref.[42] [c] $[H_2O^{II}\cdots B^-]$ and $[HO^I\cdots BH]$ are reduced and one-electron oxidized forms of the model 'water' substrate with the mass-transport characteristics of the borate base. [d] Involvement of the second H_2O molecule is implicitly included in the rate constant; involvement of 3 base species in the overall process is explained in comments in the caption to Fig. S4.

RESULTS AND DISCUSSION

Activity as a function of catalyst loading. In this study, mechanistic aspects of water electrooxidation catalyzed by non-noble transition metal oxides have been probed using very low catalyst loadings on an FTO surface. For the cobalt oxides, $[Co(EDTA)]^{2-}$ was used as a precursor for oxidative electrodeposition of CoO_x. The strong chelating ligand slows the deposition and prevents the formation of large amounts of CoO_x, but does not induce fundamental changes in the structure of the catalyst.[10] Dilute $[Ni(NH_3)_6]Cl_2$ and $Mn(CH_3COO)_2$ solutions (0.01-0.1 mM) were used to functionalize the electrodes with nickel and manganese oxides, respectively. The use of the $[Ni(NH_3)_6]Cl_2$ as a precursor decelerates NiO_x deposition[57] as needed to control the catalyst loadings for our experiments. Spontaneous adsorption of metal cations onto FTO from these solutions produced an appreciable enhancement in water electrooxidation activity and this approach was used to prepare electrodes with very low NiO_x or MnO_x surface concentrations.

Fig. 1 exemplifies d.c. cyclic voltammograms obtained with an FTO electrode modified with two different loadings for each type of a catalyst. Water electrooxidation is manifested by a steep increase in current density at potentials more positive than *ca* 1.75 V with a small level of hysteresis detected under the conditions employed. As expected, an increase in the amount of catalyst enhances the water electrooxidation capacity of the electrode.

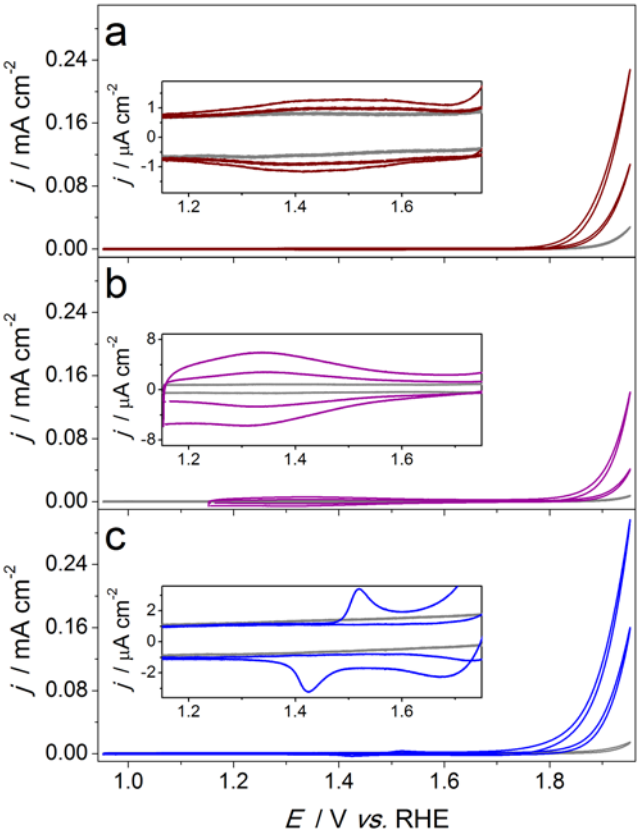

Figure 1. D.c. cyclic voltammograms ($v = 0.075$ V s^{-1}) obtained for (a) CoO_x, (b) MnO_x, and (c) NiO_x deposited at low loadings on pretreated FTO in contact with borate buffer (0.1 M, pH 9.2). For each catalyst, data for two samples having different loadings are compared with the background response from the FTO electrode (*grey*). First potential cycles are shown for CoO_x, NiO_x and background FTO cases, but the second cycle is used for MnO_x (see discussion in text for rationale). Insets highlight redox transformations of the deposited metal oxides that precede the water oxidation wave.

Prior to the catalytic process, the voltammogram for each metal oxide exhibits a fingerprint response (insets in Fig. 1) derived from redox transformations of Co, Ni or Mn oxides. These processes provide a reliable *in situ* method for quantifying the surface concentration of *electroactive* MO_x species (Γ / mol cm^{-2}). This is essential as the ultra-low loadings necessary for this study preclude visualization of catalytic species using microscopy or quantitative detection by X-ray based techniques. In the analysis that follows, the number of electrons corresponding to the processes shown in insets to Fig. 1 was assumed to be unity in each case.[11,39,46,58] On this basis, $\Gamma = Q_{Ox} / FA$, where Q_{Ox} / C is the charge associated with a one-electron oxidation of the metal oxide, $F = 96485$ C mol^{-1} and A / cm^2 is the geometric surface area of the electrode. For selected samples, the amount of deposited metal was also determined by ICP-MS (Table S2). Comparison of thus measured surface concentration of Co with Γ indicates that not more than 10% of electrodeposited CoO_x is electrochemically active, in reasonable agreement with a recent report on thicker cobalt oxide films.[46] A similarly low fraction of electrochemically active metal centers was found here for MnO_x. For the NiO_x catalyst, a substantially higher accessibility to redox transformations was established where *ca* 60-70% of deposited nickel contributed to the voltammetric signals shown in Fig. 1c inset. Previously, 100% electrochemical activity was reported for electrodeposited NiO_x based on comparisons of quartz crystal microbalance and voltammetric data.[58]

The voltammetric response for NiO_x, CoO_x and unmodified FTO was stable on the time-scale of the measurements. However, substantial and persistent degradation was found for the MnO_x catalysts during experiments, which was evident from a decrease in water oxidation current and accompanying decrease in the MnO_x process preceding the catalytic wave (see Fig. S7).

Previous reports on CoO_x-catalyzed water electrooxidation applying thicker films than considered here consistently suggest that the geometric surface-weighed activity of the electrode (A cm^{-2}) scales linearly with the surface concentration of cobalt and Γ.[11,39,59] The activity-loading dependences reported herein for CoO_x, NiO_x and MnO_x with Γ in the sub-nanomol per cm^2 range reveal distinct behaviors for each catalyst (Fig. 2). An OER overpotential of *ca* $\eta = 0.62$ V (1.853 V *vs.* RHE) was selected for comparisons of the catalytic current, $j_{0.62V}$, to limit interference from background water-oxidation catalyzed by the FTO substrate and ohmic losses.

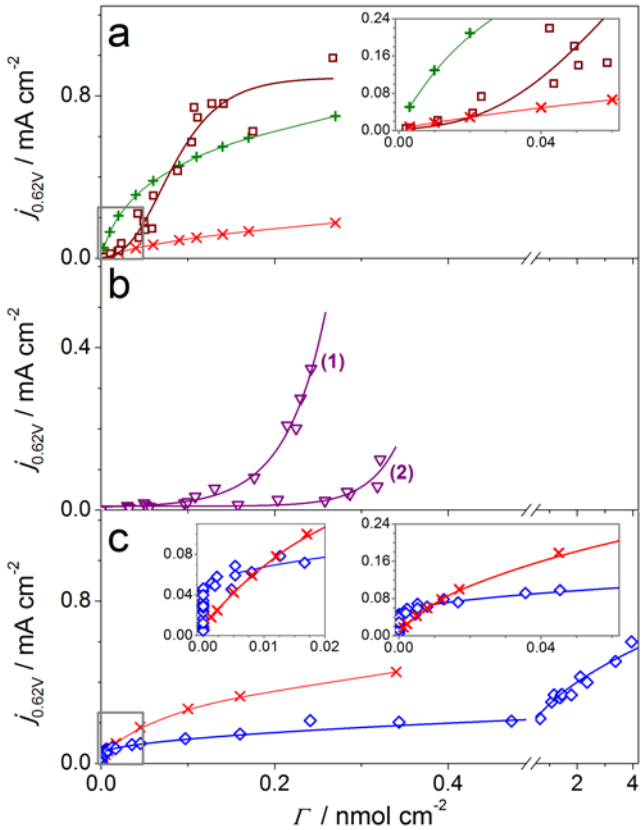

Figure 2. Dependence of d.c. water oxidation current density at 1.853 V ($\eta \approx 0.62$ V) on the surface concentration of electroactive CoO_x (a, *wine squares*), MnO_x (b, *purple triangles*) and NiO_x (c, *blue rhombuses*). Data were extracted from d.c. components of FT a.c. voltammograms measured in borate buffer (0.1 M, pH 9.2). *Green* and *red* symbols refer to theoretical predictions based on the model in Table 1 and parameters in Table 2 for Γ ranges **a** 3-11 (×), 100-110 (+), and **c** 5-10 pmol cm^{-2}. Datasets (1) and (2) in **b** were obtained with pretreated FTO supports that slightly differed in water oxidation activity (see text). Expanded versions of the low Γ regions are shown in insets. Lines are guides to an eye.

At low CoO_x coverage (Γ < 10 pmol cm^{-2}), the enhancement in water oxidation current density exceeds that predicted from a linear activity-loading dependence (see inset to Fig. 2a). Since data in Fig. 2 are not corrected for iR_u-drop, a linear relationship between the intrinsic activity of the electrode and Γ would result in a dependence of the kind derived from theoretical simulations (*vide infra* and Fig. 2). This indicates a notable increase in the specific metal-weighted catalytic activity, $i_{0.62V}$ / A nmol^{-1} = $j_{0.62V}/\Gamma$. At higher loadings, the $j_{0.62V}$ *vs.* Γ dependence trends downwards as expected if $i_{0.62V}$ is not strongly dependent on Γ, in agreement with reports for much thicker catalyst films.[11,39,59]

For MnO_x, $i_{0.62V}$ increases substantially over the whole catalyst loading range examined, but is highly sensitive to the properties of the FTO support (*cf.* datasets **1** and **2** in Fig. 2b). Dependence **1** of $j_{0.62V}$ *vs.* Γ results from the use of pretreated FTO electrodes with essentially no water oxidation activity at η = 0.62 V ($j_{0.62V} \leq 1$ μA cm^{-2}) prior to deposition of MnO_x. Dependence **2** was obtained with FTO supports pretreated in the same manner but that were slightly more active with $j_{0.62V}$ of *ca* 3-5 μA cm^{-2} before functionalization with MnO_x.

For the NiO_x electrocatalysts with extremely low loadings (Γ below a few pmol cm^{-2}), the water oxidation current densities rise dramatically with essentially undetectable increases in the amount of Ni (inset to Fig. 2c). In this ultra-low Γ range, NiO_x substantially outperforms CoO_x and especially MnO_x in terms of $i_{0.62V}$. However, higher surface concentrations of NiO_x produce lower enhancements in catalytic activity (Fig. 2c), with $i_{0.62V}$ decreasing from 2 to 0.1 A nmol^{-1} when Γ is increased from 5 to 300 pmol cm^{-2}. Once Γ exceeds 1000 pmol cm^{-2}, the activity *vs.* loading dependence for NiO_x is close to linear. The incorporation of trace Fe into NiO_x to form $FeNiO_x$ has been shown to significantly enhance the water oxidation catalytic activity.[60] Although such a process cannot be absolutely excluded herein, our control measurements with blank FTO (continuous cycling the potential from 1.15 to 2.15 V; chronoamperometry at 1.8 V) did not show any indication of Fe being deposited, *viz.* unexpected enhancement of the electrooxidation current on the timescale of our measurements.

The pronounced increase in the specific water oxidation activity at low catalyst loadings can be attributed to the crucial importance of multi-atomic metal centers (ensembles) in sustaining this reaction efficiently. Indeed, the involvement of at least two adjacent metal atoms in the oxide structure is postulated in proposed mechanisms for the OER.[5,32,36,37,46,61-63] An enhanced relative contribution of catalyst dissolution to the apparent increase in $i_{0.62V}$ may apply for low loadings of the MnO_x catalyst. Importantly, there was no detectable loss of catalytic activity observed for CoO_x and NiO_x.

A.c. voltammetric studies: qualitative mechanistic observations. Interpretations of how redox transformations of heterogeneous MO_x catalysts contribute to water electrooxidation, based on d.c. methodology, has been the subject of debate.[37,45,46,63,64] FT a.c. voltammetric analyses have provided some qualitative mechanistic insights.[48,65] The results of the more comprehensive FT a.c. voltammetric study described herein resolve ambiguities in the assignment of electron transfer processes coupled to the catalytic reaction, which are obscured in d.c. voltammetry. Detailed experiment-simulation comparisons are now introduced for the first time.

A.c. voltammetric data obtained for the CoO_x, MnO_x and NiO_x electrocatalysts in borate buffered solutions at pH 9.2 are displayed in Figs. 3 and 4. The most useful information is available from the a.c. harmonics resolved from the total current (Fig. 3a) using the FT - band filtering - inverse FT sequence of operations.[53] The aperiodic component of an FT a.c. voltammogram is analogous to a d.c. voltammogram, and is dominated by the featureless water oxidation current (Fig. 3b). However, in the a.c harmonics, the contribution from catalytic water oxidation is minimal and the underlying redox transformations become directly accessible (*cf.* Fig. 3b and 3c-d).

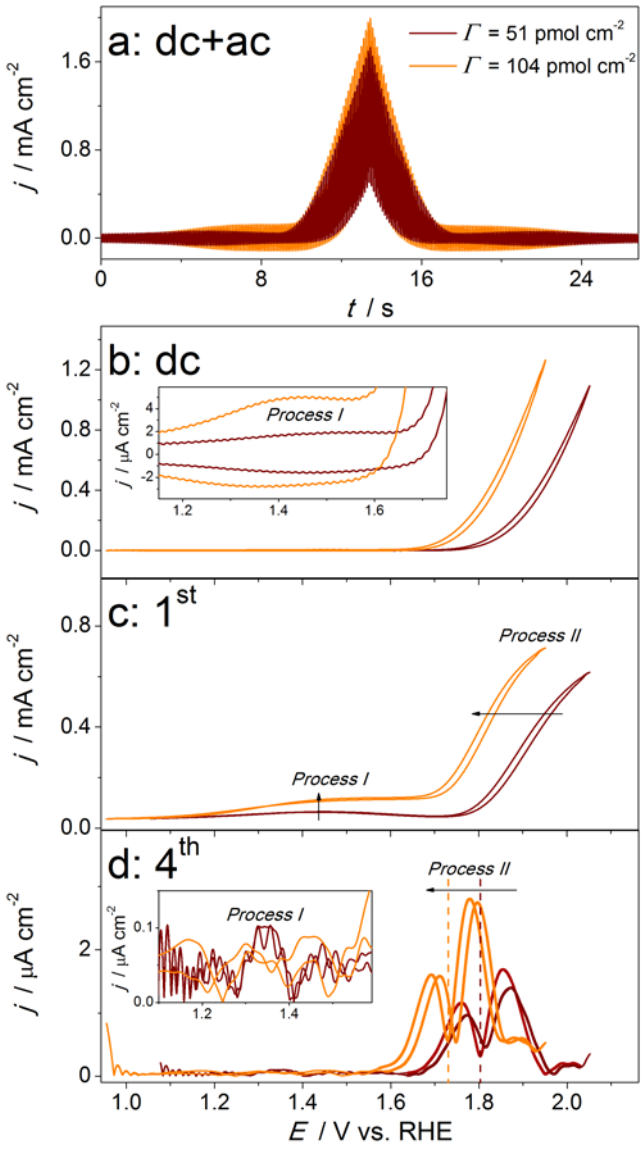

Figure 3. (a) Total a.c. plus d.c current *versus* time data, (b) resolved d.c., (c) fundamental and (d) 4th harmonic components of a.c. voltammograms (f = 9.02 Hz, ΔE = 0.080 V, v = 0.075 V s^{-1}) for water oxidation catalyzed by CoO_x at lower (*wine*) and higher (*orange*) loading. Electrolyte: 0.1 M borate buffer, pH 9.2. Arrows indicate changes in *process I* and *process II* (in panel **d**, shown as bold curves for clarity) with increase in the CoO_x surface concentration. Insets in **b** and **d** show the expanded plots for *process I*. Dashed lines in **d** define the position of *process II* in 4th harmonic on the forward (positive) d.c. potential sweep.

For the CoO_x-functionalized electrodes, the d.c. component displays the process noted above, now designated as *process I*, which precedes the catalytic wave (Fig. 3b). This is the only observable feature prior to water oxidation, and it is attributed to a $Co^{III/IV}$ transition.[64] In contrast, the fundamental a.c. harmonic exhibits two well-defined processes, *process I* and *process II*, that strongly differ in their intensity and dependence on Γ (Fig. 3c).

Variations in the CoO_x catalyst loading do not significantly affect the potential where *process I* is found (*ca* 1.4-1.5 V), but influence the current intensity in the fundamental harmonic (Fig. 3c). The electron transfer rate for this process is so slow that it is essentially indistinguishable from background in the 4th harmonic (Fig. 3d). The substantially faster *process II* gives well defined higher order harmonic signals that shift to more negative potentials and are enhanced by increases in Γ and water oxidation d.c. current density (Figs. 3c-d and 5a). Such behavior and the asymmetric shape of the harmonics for *process II* are consistent with the coupling of electron transfer to a fast chemical reaction rather than a simple electron transfer.[47,53,56,66] Thus, *process II* is coupled to a rate-limiting chemical step of the reaction and is accessible only at potentials where the catalytic current is significant, while the involvement of *process I* in efficient water oxidation catalysis is negligible.

Interpretation of the a.c. voltammetric data for MnO_x-catalyzed water oxidation is more complicated. At low Γ, there is only one clearly distinguishable and again very slow redox process prior to the onset of water electrooxidation, *process Ia*, at *ca* 1.3 V (Fig. 4a). The potential for this process is not positive enough[42] and the rate too slow to catalyze water oxidation. When Γ is above *ca* 100 pmol cm^{-2}, *process Ib* emerges in the FT a.c. voltammograms at *ca* 1.5-1.6 V (*light green* and *tan* data in Fig. 4a). The electron transfer rate for *process Ib* is faster than that for *process Ia*, as deduced from the higher current magnitude and shape of the ac harmonics (exemplified in 4th harmonics by circles over the curves in Fig. 4a). However, since there is no pronounced dependence of the position of *process Ib* on the catalyst loading and water electrooxidation rate, this redox transformation is again not regarded as being directly involved in catalysis. Finally, at even more positive potentials, the catalytically important *process II* was detected for electrodes functionalized with MnO_x and a dependence on Γ similar to that for CoO_x was observed (Figs. 4a and 5). Therefore, MnO_x-catalyzed water oxidation is predominantly governed by the kinetics of *process II* and coupled chemical transformation(s).

The a.c. voltammetric data for the NiO_x-based anodes is even more complex. At higher Γ, the d.c. components reveal a well-defined process at *ca* 1.5 V (Fig. 4b), which is prior to the catalytic wave. The corresponding fundamental a.c. harmonic shows two peaks (Fig. 4b), implying contribution from two types of redox active species. Additionally, there are substantial differences in the a.c. response on the positive and negative potential sweep (Fig. 4b and S8). These observations combined with the large peak-to-peak separation in d.c. voltammetry confirm that *processes Ia* are coupled to a structural rearrangement, such as a phase change,[31,63,67,68] rather than water oxidation, since the potential is not positive enough and is independent of the catalyst loading. Higher Γ results in the emergence of *process Ib* at *ca* 1.65-1.7 V in the a.c harmonics (Fig. 4b), as for MnO_x. *Process II* is also observed for NiO_x, though its behavior is clearly more complicated.

When examining the relationship between the catalytic current density and the position of *process II* in the fourth harmonic, the NiO_x data can be subdivided into three regions each corresponding to different catalyst loadings (Fig. 5c). At very low Γ, *process II* moves to more negative potentials as the NiO_x loading is increased and there is a concomitant improvement in catalytic activity (Fig. 5c, filled rhombuses). Once Γ reaches a level allowing both *processes Ia* and *Ib* to be detectable, *process II* is only weakly dependent on the Ni concentration/activity in the higher order a.c. components. Specifically, in the 4th harmonic, *process II* shows only a minor negative shift in potential as $j_{0.62V}$ increases from 0.05 to 0.2 mA cm^{-2} (Fig. 5c, empty rhombuses). For CoO_x and MnO_x, a shift of *ca* 0.1 V was observed for comparable increases in $j_{0.62V}$. When the NiO_x Γ is further increased, *processes Ib* and *II* merge in the higher harmonics (Fig. 4b: 4th), giving rise to highly scattered data (Fig. 5c, struck-through rhombuses). Thus, at very low NiO_x surface concentrations, water oxidation catalysis is mainly coupled to *process II*, as for CoO_x and MnO_x. However, at intermediate NiO_x loadings (5 - 500 pmol cm^{-2}) a contribution to catalysis from *process Ib* cannot be excluded. At Γ above *ca* 500 pmol cm^{-2}, *process II* shows a notable negative shift, but overlaps with *process Ib* and becomes unresolved. However, the response for *process II* can still be monitored in the fundamental harmonic over all loadings and it consistently shifts to less positive potentials as Γ increases (Fig. 4b: 1st).

In summary, FT a.c. voltammetric analysis indicates that water electrooxidation catalyzed by CoO_x, MnO_x and to a major extent by NiO_x occurs *via* a similar mechanism. On a qualitative level, *process II* and coupled chemical transformation(s) control the overall reaction rate. Interestingly, closely related FT a.c voltammetric data are obtained for non-functionalized FTO (Fig. S2b and S9), indicating that the reaction mechanism is also the same. It is also important to note that Co, Mn and Ni oxides undergo redox transformations at positive potentials prior to *process II* (Figs. 4 and 5), which suggests that that the catalytically relevant state of their surface is formed through oxidation and accompanying processes.

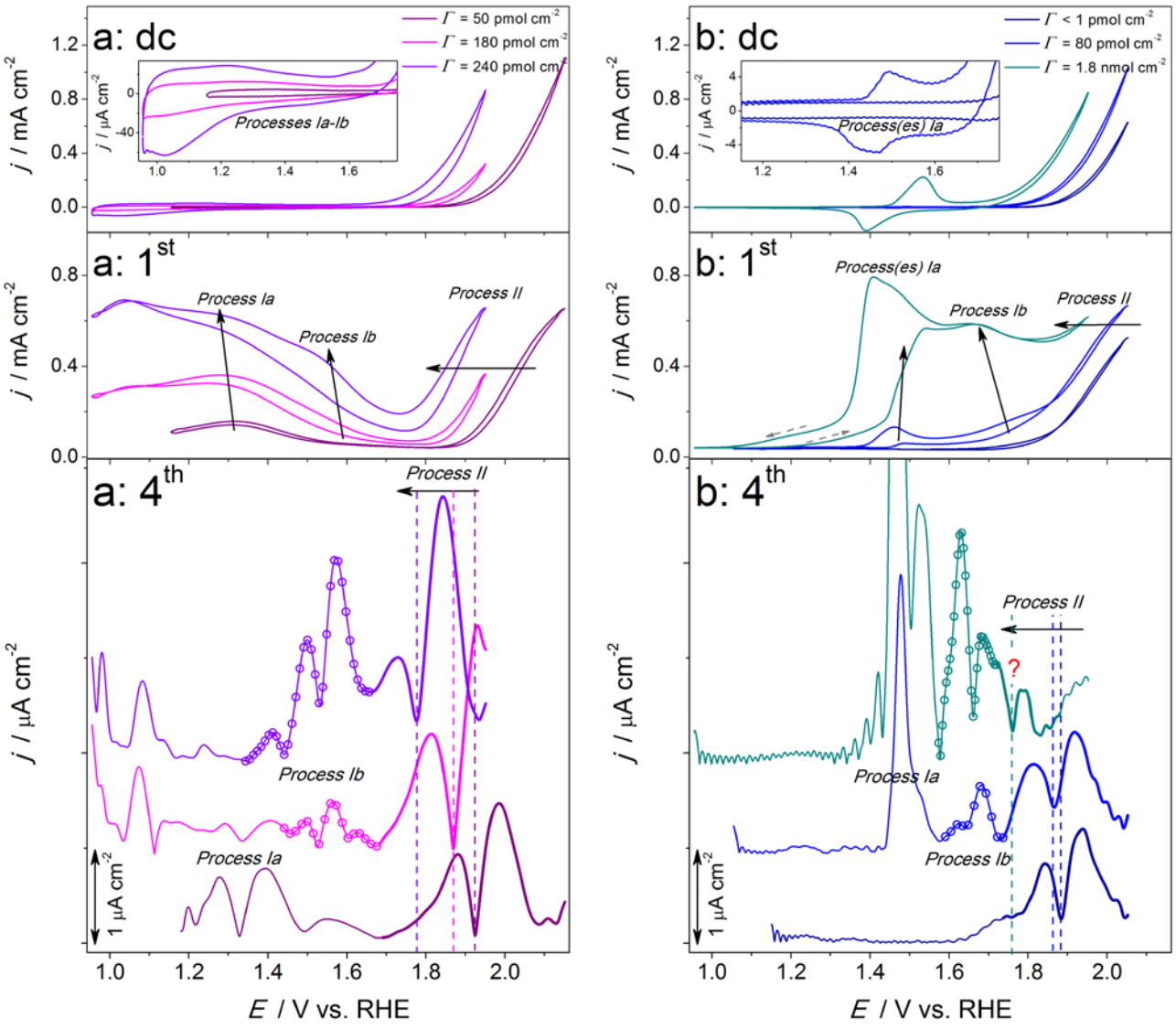

Figure 4. D.c., fundamental and 4th harmonic components of a.c. voltammograms (f= 9.02 Hz, ΔE = 0.080 V, v = 0.075 V s^{-1}) for water oxidation catalyzed by (a) MnO_x and (b) NiO_x. Insets show expanded plots for *process(es) I*. Solid arrows show changes in *processes* with increase in catalyst loading. Dashed arrows in **b: 1st** show the direction of the d.c. potential sweep. For 4th harmonics: only positive sweeps are shown for clarity; bold parts of the curves show *process II* and circles show *process Ib*; dashed lines define the position of *process II* discussed in the text.

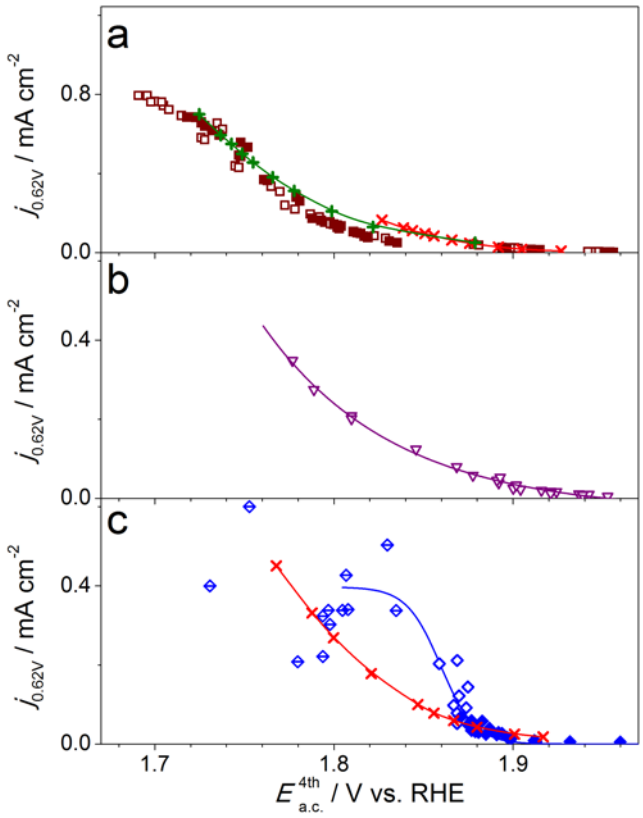

Figure 5. Dependence of the water oxidation current density at 1.853 V ($\eta \approx 0.62$ V) on the potential of *process II* in 4th a.c. harmonic (Figs. 3 and 4) for CoO_x (a, *squares*), MnO_x (b, *triangles*) and NiO_x (c, *rhombuses*). In **a**, empty and filled squares show data for positive and negative potential sweep, respectively. In **c**, variation in Γ is displayed as filled ($\Gamma \leq 5$ pmol cm^{-2}), empty (5 pmol cm^{-2} $< \Gamma \leq$ 500 pmol cm^{-2}), and struck-through rhombuses ($\Gamma >$ 500 pmol cm^{-2}). *Green* and *red* data were simulated using model in Table 1 and parameters in Table 2 for Γ (a) 3-11 (×), 100-110 (+), and (b) 5-10 pmol cm^{-2}. Lines are guides to an eye.

Experiment-simulation comparisons by FT a.c. voltammetry. The 'molecular catalysis' model used for simulations is summarized in Table 1. Three parameters need to be determined from comparisons of theoretical and experimental data: the effective reversible potential (E^0_{cat}) and the heterogeneous electron transfer rate constant (k^0_{cat}) for reaction 3, and the forward rate constant for reaction 4 (k^f). Quantitative analysis of a mechanism coupling an electron transfer process to a chemical reaction is among the most challenging problems in contemporary electrochemistry. Indeed, essentially indistinguishable d.c. voltammetric curves can be simulated using a model in Table 1 and an infinite number of combinations of the E^0_{cat}, k^0_{cat} and k^f parameters. From this perspective, FT a.c. voltammetry affords important advantages as shown previously,[47] and below.

Application of the model in Table 1 resulted in excellent agreement between a.c. voltammetric experimental data and simulations (Figs. 6 and S10) when using the parameters summarized in Tables 2 and S3. Importantly, the simulated a.c harmonic components were very sensitive to variation in the values of E^0_{cat}, k^0_{cat} and especially k^f (Fig. S11). The derived values of E^0_{cat}, k^0_{cat} and k^f allow the CoO_x, NiO_x and MnO_x catalysts to be compared quantitatively.

Hysteresis in the d.c. component and corresponding positive shift in the a.c. signals upon reversing the scan direction (Figs. 3, 6 and S12) was essentially impossible to mimic. Our modeling suggests that this hysteresis is not due to depletion of base near the electrode surface. Even at very low water oxidation current densities, when mass-transport limitations are negligible, stirring the solution does not eliminate the hysteresis (Fig. S13a). We conclude that the electrocatalytic activity of CoO_x and NiO_x changes with the applied potential, but the catalyst is returned to its previous state during the reverse voltammetric sweep, *i.e.* this change is reversible (Fig. S13b). The scan direction hysteresis is least pronounced for the lowest loadings of CoO_x and NiO_x (*cf.* data in Tables 2 and S3).

Table 2. Summary of parameters of the water electrooxidation model derived from experiment-simulation FT a.c. voltammetric comparisons.[a]

Catalyst	Γ / pmol cm^{-2}	E^0_{cat} / V *vs.* RHE	k^0_{cat} / s^{-1}	10^{-4} k^f / M^{-1} s^{-1}
CoO_x	3-11	2.00 ± 0.01	100 ± 10	3.9 ± 0.3
	40-50	1.94 ± 0.01	90 ± 10	8 ± 4
	100-110	1.94 ± 0.02	320 ± 20	35 ± 4
NiO_x	0.5-1.5	1.99 ± 0.01	1750 ± 100	66 ± 10
	5-10	2.01 ± 0.01	600 ± 40	28 ± 4
MnO_x	50-55	2.09 ± 0.02	77 ± 3	6.8 ± 0.7
	130	2.08	127	6.7
	210	2.03	110	8.2

[a] Mean values and standard deviations derived from best fits of theory to 2-4 experimental datasets for the negative potential direction voltammetric sweep. For MnO_x, one dataset was analyzed for each Γ entry except for Γ = 50-55 pmol cm^{-2}.

At high Γ, unrealistically low k^0_{cat} and k^f would be required to fit the positive sweep, *i.e.* values that would not allow the experimentally observed peak currents in d.c. voltammetry (Fig. S3) to be reached. Similarly, no acceptable fit for the positive sweep could be achieved for MnO_x at high Γ (Table S3). On this basis, it can be argued that the voltammetric data obtained during the backward (negative) sweep provides a better reflection of the catalytic properties relevant to water electrooxidation.

Several important conclusions can be drawn on the basis of the parameters derived from fitting simulations to experimental data (Table 2). The effective reversible potentials for the CoO_x, NiO_x and MnO_x redox transformations coupled to substrate oxidation in solution are similar. Our analysis suggests that E^0_{cat} lies in the 1.9-2.1 V *vs.* RHE potential range and is not strongly dependent on Γ. This agrees with the lower limit for E^0_{cat} value for CoO_x of >1.92 *vs.* RHE reported by the group of Savéant and Costentin.[46] The similarity of E^0_{cat} for CoO_x, NiO_x and MnO_x provides one fundamental explanation for each being good water oxidation catalysts with comparable activity. If one considers a 'heterogeneous catalysis' model (Table S2), similar E^0_{cat} values reflect a similar strength of adsorption of the substrate on the catalyst surface.

The dependence of the CoO_x catalyst properties on Γ is reflected by the need to employ catalyst loading dependent [E^0_{cat}, k^0_{cat}, k^f] parameter combinations to fit the experimentally observed $j_{0.62V}$ *vs.* Γ and $j_{0.62V}$ *vs.* E^{4th}_{ac} data (Fig. 2a; Fig. 5; Table 2). Successful mod-

eling of the data at higher Γ required higher k^f and k^0_{cat} values (Table 2). An increase in k^f at higher catalyst concentrations is consistent with an 'ensemble effect', reflecting the critical importance of multi-atomic active sites. A similar, but less pronounced effect of Γ on the k^f and k^0_{cat} values was found for MnO_x. Deterioration of the NiO_x specific activity as the loading increases is also reflected in a lowering of k^f and k^0_{cat} values (Table 2). A plausible reason for the deceleration in k^0_{cat} is bulk structural rearrangement that occurs upon oxidation/reduction of the nickel oxide.[31,63,68]

The values of k^f for CoO_x, NiO_x and MnO_x are of the same order of magnitude and fall within the 4×10^4 to 8×10^5 M^{-1} s^{-1} range. Previous works aimed at parameterizing the catalytic reaction between the oxidized, active state of CoO_x[45,46] or MnO_x[32] and H_2O used a pseudo-first-order rate constant, k^f_1 / s^{-1}. Thus, comparisons with our results can be made by multiplying the second order rate constant, k^f, by the concentration of base to give $k^f C_B$. The lower limits for $k^f_1 \geq 2$ s^{-1} and ≥ 112.5 s^{-1} reported by the groups of Bard[45] and Savéant,[46] respectively, are consistent with the values of $k^f C_B$ (17500 s^{-1}) derived from our analysis of the CoO_x a.c voltammetric data (Table 2). For MnO_x, the $k^f C_B$ rate determined herein is *ca* 4000 s^{-1}, which is in agreement with a lower limit of 100 s^{-1} reported by Dau and colleagues and notably higher than $k^f_1 = 500$ s^{-1} for the Mn_4CaO_5 complex of Photosystem-II.[32,69]

Considering other influential catalysts, molecular Ru complexes have been studied in great detail.[70] The k^f_1 rate constants of 0.00075 and 0.0014 s^{-1} for Ru monomers ($[Ru^{II}(tpy)(bpm)(OH_2)]^{2+}$, $[Ru^{II}(tpy)(bpz)(OH_2)]^{2+}$),[71] and 0.002 s^{-1} for the 'blue dimer' (*cis,cis*-$[(bpy)_2(H_2O)Ru^{III}O Ru^{III}(OH_2)(bpy)_2]^{4+}$),[72] were reported. Values of k^f_1 ranging from 0.00014 to 0.00078 s^{-1} were determined for a series of other Ru monomers and dimers,[73] while values up to 0.014 s^{-1} have been reported for the $[Ru_2^{II}(bpp)(trpy)(H_2O)_2]^{3+}$ dimer.[74] All are several orders of magnitude lower than k^f_1 for the more efficient heterogeneous systems examined in this and other studies.

Another important outcome of our work is the exceptionally high specific catalytic activity of nickel oxides at ultra-low loadings that substantially surpasses that of CoO_x and MnO_x (Table 2). In particular, at the lowest voltammetrically detectable Γ of *ca* 1 pmol cm^{-2}, k^f and k^0_{cat} for the NiO_x-modified electrodes are an order of magnitude higher than those for CoO_x with loadings below 50 pmol cm^{-2}. One strategy to exploit this property of NiO_x is to immobilize the catalyst on a very high-surface area support to avoid the formation of dense nickel oxide layers since they exhibit notably lower specific activity.

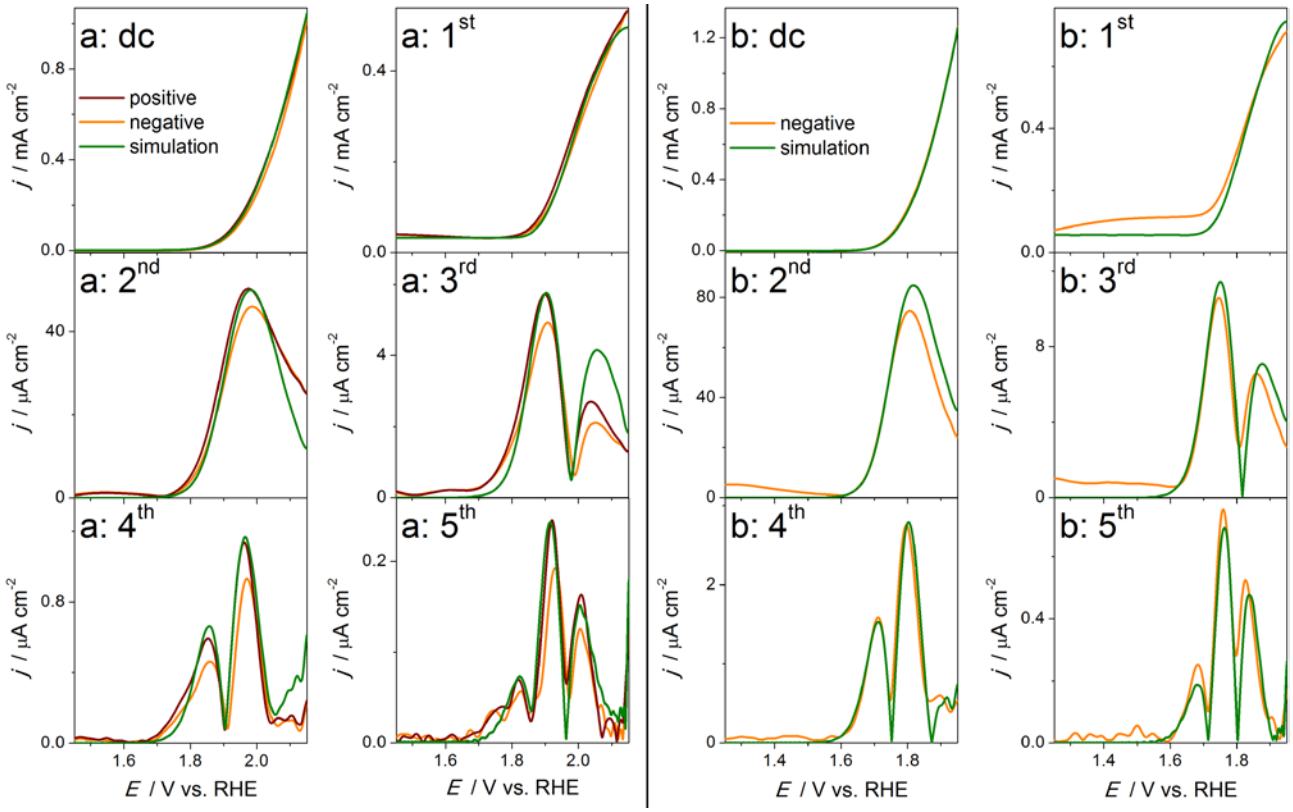

Figure 6. Comparison of experimental (positive sweep in *wine*; negative sweep in *orange*) and simulated (*green*) FT a.c. voltammetric data for water electrooxidation catalyzed by CoO_x with Γ of (a) 11 and (b) 104 pmol cm^{-2}. Experimental conditions are as in Fig. 3. Simulations are based on model in Table 1 and $E^0_{cat} = 2.00$ (a) and 2.01 V (b), $k^0_{cat} = 110$ (a) and 325 s^{-1} (b), $k^f = 35.8\times10^4$ (a) and 35.9×10^4 M s^{-1} (b). Note that experimental and simulated data are often indiscernible.

CONCLUSIONS

Systematic examination of water electrooxidation catalyzed by low amounts of cobalt, manganese and nickel oxides using FT a.c. voltammetry enables unique mechanistic insights and quantification of key reaction parameters. The experimental data are reliably mimicked by the 'molecular catalysis' model and the E^0_{cat}, k^0_{cat}, and k^f parameters have been derived *via* extensive experiment-simulation comparisons. Estimates of the pseudo-first order k^f provided by our analysis are substantially higher than values reported previously for similar and other water oxidation catalysts. This suggests that FT a.c. voltammetry offers improvements in sensitivity exploitable in quantitative kinetic studies of this complex reaction. The unprecedentedly high specific catalytic activity of NiO_x at very low loadings (<2 pmol cm^{-2}), as reflected by high k^f and k^0_{cat}, could be of applied significance.

Quantitative FT ac. voltammetric studies can significantly improve our understanding of mechanistic aspects of water electrooxidation. The parameterized electrode model of the reaction introduced here for the first time provides a guide for *in situ* spectroscopic studies to assist in identification of true active states of metal-oxide-based electrocatalysts, and indicates that experiments at very positive applied potential (1.9-2.1 V vs RHE) are desirable. Information derived from these experiments is indispensable for the design and benchmarking of improved catalytic materials for this critically important process.

ASSOCIATED CONTENT

Supporting Information. Fig. S1: Photographs of electrodes; Fig. S2: a.c. voltammetry for FTO; Fig. S3: d.c. voltammetric peak current data for FTO; Fig. S4: DigiElch 7.0F parameters; Fig. S5: modeling of two non-interacting water oxidation catalysts; Table S1: 'heterogeneous catalysis' model; Fig. S6: similarity of predictions of the 'molecular' and 'heterogeneous' catalysis models; Table S2: ICP-MS data; Fig. S7: d.c. voltammetry for MnO_x; Fig. S8: higher harmonics of FT a.c. voltammogram for NiO_x; Fig. S9: $j_{0.72V}$ *vs.* $E^{4th}_{a.c.}$ plot for FTO; Fig. S10: experiment-simulation comparisons for NiO_x; Fig. S11: influence of k^0_{cat}, E^0_{cat}, and k^f on simulated FT a.c. voltammograms; Fig. S12: experiment-simulation comparisons for CoO_x; Table S3: 'molecular catalysis' model parameters derived from the forward voltammetric sweep data. Fig. S13: effect of stirring and multiple cycling on d.c. voltammetry for water oxidation. This material is available free of charge via the Internet at http://pubs.acs.org.

AUTHOR INFORMATION

Corresponding Author

* E-mail for L.S.: leone.spiccia@monash.edu
E-mail for A.N.S.: alexandr.simonov@monash.edu;

Funding Sources

Australian Research Council Centre of Excellence for Electromaterials Science (ACES).

ACKNOWLEDGMENT

The authors gratefully acknowledge the use of facilities in the Monash Centre for Electron Microscopy (MCEM), and the Australian Research Council for financial support.

REFERENCES

(1) Lewis, N. S.; Nocera, D. G. *Proc. Natl. Acad. Sci. U. S. A.* **2006**, *103*, 15729.
(2) Lewis, N. S. *Science* **2016**, *351*, aad1920.
(3) Faunce, T.; Styring, S.; Wasielewski, M. R.; Brudvig, G. W.; Rutherford, A. W.; Messinger, J.; Lee, A. F.; Hill, C. L.; deGroot, H.; Fontecave, M.; MacFarlane, D. R.; Hankamer, B.; Nocera, D. G.; Tiede, D. M.; Dau, H.; Hillier, W.; Wang, L.; Amal, R. *Energy Environ. Sci.* **2013**, *6*, 1074.
(4) Bard, A. J.; Fox, M. A. *Acc. Chem. Res.* **1995**, *28*, 141.
(5) Dau, H.; Limberg, C.; Reier, T.; Risch, M.; Roggan, S.; Strasser, P. *ChemCatChem* **2010**, *2*, 724.
(6) McCrory, C. C. L.; Jung, S.; Ferrer, I. M.; Chatman, S. M.; Peters, J. C.; Jaramillo, T. F. *Journal of the American Chemical Society* **2015**, *137*, 4347.
(7) Kanan, M. W.; Nocera, D. G. *Science* **2008**, *321*, 1072.
(8) Nocera, D. G. *Acc. Chem. Res.* **2012**, *45*, 767.
(9) Cobo, S.; Heidkamp, J.; Jacques, P.-A.; Fize, J.; Fourmond, V.; Guetaz, L.; Jousselme, B.; Ivanova, V.; Dau, H.; Palacin, S.; Fontecave, M.; Artero, V. *Nature Mater.* **2012**, *11*, 802.
(10) Bonke, S. A.; Wiechen, M.; Hocking, R. K.; Fang, X.-Y.; Lupton, D. W.; MacFarlane, D. R.; Spiccia, L. *ChemSusChem* **2015**, *8*, 1394.
(11) Klingan, K.; Ringleb, F.; Zaharieva, I.; Heidkamp, J.; Chernev, P.; Gonzalez-Flores, D.; Risch, M.; Fischer, A.; Dau, H. *ChemSusChem* **2014**, *7*, 1301.
(12) Dinca, M.; Surendranath, Y.; Nocera, D. G. *Proc. Natl. Acad. Sci. U. S. A.* **2010**, *107*, 10337.
(13) Risch, M.; Klingan, K.; Heidkamp, J.; Ehrenberg, D.; Chernev, P.; Zaharieva, I.; Dau, H. *Chem. Commun.* **2011**, *47*, 11912.
(14) Görlin, M.; Chernev, P.; Ferreira de Araújo, J.; Reier, T.; Dresp, S.; Paul, B.; Krähnert, R.; Dau, H.; Strasser, P. *J. Am. Chem. Soc.* **2016**, *138*, 5603.
(15) Hocking, R. K.; Brimblecombe, R.; Chang, L. Y.; Singh, A.; Cheah, M. H.; Glover, C.; Casey, W. H.; Spiccia, L. *Nature Chem.* **2011**, *3*, 461.
(16) Zhou, F. L.; Izgorodin, A.; Hocking, R. K.; Spiccia, L.; MacFarlane, D. R. *Adv. Energy Mater.* **2012**, *2*, 1013.
(17) Zaharieva, I.; Najafpour, M. M.; Wiechen, M.; Haumann, M.; Kurz, P.; Dau, H. *Energy Environ. Sci.* **2011**, *4*, 2400.
(18) Zaharieva, I.; Chernev, P.; Risch, M.; Klingan, K.; Kohlhoff, M.; Fischer, A.; Dau, H. *Energy Environ. Sci.* **2012**, *5*, 7081.
(19) Fekete, M.; Hocking, R. K.; Chang, S. L. Y.; Italiano, C.; Patti, A. F.; Arena, F.; Spiccia, L. *Energy Environ. Sci.* **2013**, *6*, 2222.
(20) Singh, A.; Hocking, R. K.; Chang, S. L. Y.; George, B. M.; Fehr, M.; Lips, K.; Schnegg, A.; Spiccia, L. *Chem. Mater.* **2013**, *25*, 1098.
(21) Huynh, M.; Bediako, D. K.; Nocera, D. G. *Journal of the American Chemical Society* **2014**, *136*, 6002.
(22) Huynh, M.; Shi, C.; Billinge, S. J. L.; Nocera, D. G. *J. Am. Chem. Soc.* **2015**, *137*, 14887.
(23) González-Flores, D.; Zaharieva, I.; Heidkamp, J.; Chernev, P.; Martínez-Moreno, E.; Pasquini, C.; Mohammadi, M. R.; Klingan, K.; Gernet, U.; Fischer, A.; Dau, H. *ChemSusChem* **2015**, *9*, 379.
(24) Gorlin, Y.; Lassalle-Kaiser, B.; Benck, J. D.; Gul, S.; Webb, S. M.; Yachandra, V. K.; Yano, J.; Jaramillo, T. F. *J. Am. Chem. Soc.* **2013**, *135*, 8525.
(25) Chang, S. L. Y.; Singh, A.; Hocking, R. K.; Dwyer, C.; Spiccia, L. *J. Mater. Chem. A* **2014**, *2*, 3730.
(26) Hocking, R. K.; King, H. J.; Hesson, A.; Bonke, S. A.; Johannessen, B.; Fekete, M.; Spiccia, L.; Chang, S. L. Y. *Aust. J. Chem.* **2015**, *68*, 1715.
(27) Kanan, M. W.; Yano, J.; Surendranath, Y.; Dinca, M.; Yachandra, V. K.; Nocera, D. G. *J. Am. Chem. Soc.* **2010**, *132*, 13692.
(28) Bediako, D. K.; Lassalle-Kaiser, B.; Surendranath, Y.; Yano, J.; Yachandra, V. K.; Nocera, D. G. *J. Am. Chem. Soc.* **2012**, *134*, 6801.
(29) Risch, M.; Khare, V.; Zaharieva, I.; Gerencser, L.; Chernev, P.; Dau, H. *J. Am. Chem. Soc.* **2009**, *131*, 6936.
(30) Risch, M.; Ringleb, F.; Kohlhoff, M.; Bogdanoff, P.; Chernev, P.; Zaharieva, I.; Dau, H. *Energy Environ. Sci.* **2015**, *8*, 661.

(31) Yoshida, M.; Mitsutomi, Y.; Mineo, T.; Nagasaka, M.; Yuzawa, H.; Kosugi, N.; Kondoh, H. *J. Phys. Chem. C* **2015**, *119*, 19279.
(32) Zaharieva, I.; Gonzalez-Flores, D.; Asfari, B.; Pasquini, C.; Mohammadi, M. R.; Klingan, K.; Zizak, I.; Loos, S.; Chernev, P.; Dau, H. *Energy Environ. Sci.* **2016**, *9*, 2433.
(33) Wiechen, M.; Najafpour, M. M.; Allakhverdiev, S. I.; Spiccia, L. *Energy. Environ. Sci.* **2014**, *7*, 2203.
(34) Surendranath, Y.; Dinca, M.; Nocera, D. G. *J. Am. Chem. Soc.* **2009**, *131*, 2615.
(35) Reece, S. Y.; Hamel, J. A.; Sung, K.; Jarvi, T. D.; Esswein, A. J.; Pijpers, J. J. H.; Nocera, D. G. *Science* **2011**, *334*, 645.
(36) Surendranath, Y.; Kanan, M. W.; Nocera, D. G. *J. Am. Chem. Soc.* **2010**, *132*, 16501.
(37) Bediako, D. K.; Costentin, C.; Jones, E. C.; Nocera, D. G.; Savéant, J.-M. *J. Am. Chem. Soc.* **2013**, *135*, 10492.
(38) Surendranath, Y.; Lutterman, D. A.; Liu, Y.; Nocera, D. G. *J. Am. Chem. Soc.* **2012**, *134*, 6326.
(39) Esswein, A. J.; Surendranath, Y.; Reece, S. Y.; Nocera, D. G. *Energy Environ. Sci.* **2011**, *4*, 499.
(40) McAlpin, J. G.; Surendranath, Y.; Dinca, M.; Stich, T. A.; Stoian, S. A.; Casey, W. H.; Nocera, D. G.; Britt, R. D. *J. Am. Chem. Soc.* **2010**, *132*, 6882.
(41) Nørskov, J. K.; Bligaard, T.; Hvolbaek, B.; Abild-Pedersen, F.; Chorkendorff, I.; Christensen, C. H. *Chem. Soc. Rev.* **2008**, *37*, 2163.
(42) Man, I. C.; Su, H.-Y.; Calle-Vallejo, F.; Hansen, H. A.; Martínez, J. I.; Inoglu, N. G.; Kitchin, J.; Jaramillo, T. F.; Nørskov, J. K.; Rossmeisl, J. *ChemCatChem* **2011**, *3*, 1159.
(43) Bajdich, M.; García-Mota, M.; Vojvodic, A.; Nørskov, J. K.; Bell, A. T. *Journal of the American Chemical Society* **2013**, *135*, 13521.
(44) Friebel, D.; Louie, M. W.; Bajdich, M.; Sanwald, K. E.; Cai, Y.; Wise, A. M.; Cheng, M.-J.; Sokaras, D.; Weng, T.-C.; Alonso-Mori, R.; Davis, R. C.; Bargar, J. R.; Nørskov, J. K.; Nilsson, A.; Bell, A. T. *J. Am. Chem. Soc.* **2015**, *137*, 1305.
(45) Ahn, H. S.; Bard, A. J. *Journal of the American Chemical Society* **2015**, *137*, 612.
(46) Costentin, C.; Porter, T. R.; Savéant, J.-M. *Journal of the American Chemical Society* **2016**, *138*, 5615.
(47) Simonov, A. N.; Morris, G. P.; Mashkina, E.; Bethwaite, B.; Gillow, K.; Baker, R. E.; Gavaghan, D. J.; Bond, A. M. *Anal. Chem.* **2016**, *88*, 4724.
(48) Guo, S.-X.; Liu, Y.; Bond, A. M.; Zhang, J.; Esakki Karthik, P.; Maheshwaran, I.; Senthil Kumar, S.; Phani, K. L. N. *Phys. Chem. Chem. Phys.* **2014**, *16*, 19035.
(49) Adamson, H.; Simonov, A. N.; Kierzek, M.; Rothery, R. A.; Weiner, J. H.; Bond, A. M.; Parkin, A. *Proc. Natl. Acad. Sci. U. S. A.* **2015**, *112*, 14506.
(50) Bhat, T. R.; Krishnamurthy, M. *J. Inorg. Nucl. Chem.* **1963**, *25*, 1147.
(51) Glemser, O. In *Handbook of Preparative Inorganic Chemistry (Second Edition)*; Academic Press: 1965, p 1545.
(52) Gans, P.; Gill, J. B.; Johnson, L. H. *J. Chem. Soc., Dalton Trans. (1972-1999)* **1993**, 345.
(53) Bond, A. M.; Elton, D.; Guo, S.-X.; Kennedy, G. F.; Mashkina, E.; Simonov, A. N.; Zhang, J. *Electrochem. Commun.* **2015**, *57*, 78.
(54) ElchSoft http://www.elchsoft.com/digielch/DigiElch7
(55) Simonov, A. N.; Morris, G. P.; Mashkina, E. A.; Bethwaite, B.; Gillow, K.; Baker, R. E.; Gavaghan, D. J.; Bond, A. M. *Anal. Chem.* **2014**, *86*, 8408.
(56) Bond, A. M.; Mashkina, E. A.; Simonov, A. N. In *Developments in Electrochemistry*; John Wiley & Sons, Ltd: 2014, p 21.
(57) Singh, A.; Chang, S. L. Y.; Hocking, R. K.; Bach, U.; Spiccia, L. *Energy & Environmental Science* **2013**, *6*, 579.
(58) Trotochaud, L.; Ranney, J. K.; Williams, K. N.; Boettcher, S. W. *Journal of the American Chemical Society* **2012**, *134*, 17253.
(59) Farrow, C. L.; Bediako, D. K.; Surendranath, Y.; Nocera, D. G.; Billinge, S. J. L. *Journal of the American Chemical Society* **2013**, *135*, 6403.
(60) Trotochaud, L.; Young, S. L.; Ranney, J. K.; Boettcher, S. W. *J. Am. Chem. Soc.* **2014**, *136*, 6744.
(61) McAlpin, J. G.; Stich, T. A.; Ohlin, C. A.; Surendranath, Y.; Nocera, D. G.; Casey, W. H.; Britt, R. D. *J. Am. Chem. Soc.* **2011**, *133*, 15444.
(62) Dau, H.; Haumann, M. *Coord. Chem. Rev.* **2008**, *252*, 273.
(63) Smith, R. D. L.; Sherbo, R. S.; Dettelbach, K. E.; Berlinguette, C. P. *Chem. Mater.* **2016**, *28*, 5635.
(64) Gerken, J. B.; McAlpin, J. G.; Chen, J. Y. C.; Rigsby, M. L.; Casey, W. H.; Britt, R. D.; Stahl, S. S. *J. Am. Chem. Soc.* **2011**, *133*, 14431.
(65) Liu, Y.; Guo, S.-X.; Ding, L.; Ohlin, C. A.; Bond, A. M.; Zhang, J. *ACS Appl. Mater. Interfaces* **2015**, *7*, 16632.
(66) Abdul-Rahim, O.; Simonov, A. N.; Rüther, T.; Boas, J. F.; Torriero, A. A. J.; Collins, D. J.; Perlmutter, P.; Bond, A. M. *Anal. Chem.* **2013**, *85*, 6113.
(67) Alsabet, M.; Grden, M.; Jerkiewicz, G. *Electrocatalysis* **2014**, *5*, 136.
(68) Alsabet, M.; Grdeń, M.; Jerkiewicz, G. *Electrocatalysis* **2015**, *6*, 60.
(69) Klauss, A.; Haumann, M.; Dau, H. *J. Phys. Chem. B* **2015**, *119*, 2677.
(70) Concepcion, J. J.; Jurss, J. W.; Brennaman, M. K.; Hoertz, P. G.; Patrocinio, A. O. T.; Murakami Iha, N. Y.; Templeton, J. L.; Meyer, T. J. *Acc. Chem. Res.* **2009**, *42*, 1954.
(71) Concepcion, J. J.; Jurss, J. W.; Templeton, J. L.; Meyer, T. J. *J. Am. Chem. Soc.* **2008**, *130*, 16462.
(72) Gersten, S. W.; Samuels, G. J.; Meyer, T. J. *J. Am. Chem. Soc.* **1982**, *104*, 4029.
(73) Zong, R.; Thummel, R. P. *J. Am. Chem. Soc.* **2005**, *127*, 12802.
(74) Sens, C.; Romero, I.; Rodríguez, M.; Llobet, A.; Parella, T.; Benet-Buchholz, J. *J. Am. Chem. Soc.* **2004**, *126*, 7798.

SYNOPSIS TOC